Research Square

Preprints are preliminary reports that have not undergone peer review.
They should not be considered conclusive, used to inform clinical practice,
or referenced by the media as validated information.

Development of an Experimental Test Bed for Cryogenic Propellant Regeneration In Orbit

Cameron Leslie

cameron.leslie@cranfield.ac.uk

Cranfield University

Stephen Hobbs

Cranfield University

Enric Grustan-Gutiérrez

Cranfield University

Research Article

Keywords: Atmosphere-breathing Electric Propulsion, ABEP, Cryogenic Propellant Regeneration

Posted Date: November 9th, 2026

DOI: https://doi.org/10.21203/rs.3.rs-11224936/v1

License: This work is licensed under a Creative Commons Attribution 4.0 International License.
Read Full License

Additional Declarations: No competing interests reported.

Development of an Experimental Test Bed for Cryogenic Propellant Regeneration In Orbit

Cameron Leslie[1*], Stephen Hobbs[1] and Enric Grustan-Gutiérrez[1*]

[1*]Faculty of Engineering & Applied Science, Cranfield University, College Road, Cranfield, MK43 0AL, Bedfordshire, United Kingdom.

*Corresponding author(s). E-mail(s): cameron.leslie@cranfield.ac.uk; e.grustan@cranfield.ac.uk;

Abstract

Atmosphere-breathing electric propulsion (ABEP) enables spacecraft to use gases collected in orbit as propellant, supporting sustained operations at low altitudes and improving observation and communication missions. Recent studies have proposed using cryogenic pumps to improve the compression performance of ABEP intakes. This work explores using cryopumps to enable an alternative ABEP architecture, where gases are collected and stored independently prior to being used for thrust. We present progress on PHROST (Propellant Harvesting of Rarefied gases in Orbit for Supplying electric Thrusters), an experimental test bed for studying cryogenic propellant regeneration. Firstly, key component designs, subsystem selections, and a methodology for creating a representative intake environment are shown. Then, simulations of molecular flow and radiation heat transfer inside the pump are used to establish design feasibility during the collection phase. Finally, ongoing development is summarised.

Keywords: Atmosphere-breathing Electric Propulsion, ABEP, Cryogenic Propellant Regeneration

1 Introduction

Very low Earth orbit (VLEO) offers significant advantages to observation and communication missions [1]. For example, observation payloads benefit from closer proximity to Earth's surface by enabling higher resolution imagery. While communication payloads benefit from the shorter distance to ground stations by reducing losses incurred

during transmission. However, lower altitudes come at the cost of increased atmospheric drag. Atmosphere-breathing electric propulsion (ABEP) offers the ability to overcome these forces by using the rarefied gases encountered in VLEO as an in-situ propellant source [2–5]. In its simplest form, ABEP systems collect the incoming gases, ionise them, and accelerate them to produce thrust. The primary objective of most recent ABEP concepts is to generate enough thrust to overcome aerodynamic drag, thereby enabling long term operations in VLEO without the need to launch with a finite supply of propellant.

More recently, concepts have explored building on ABEP with active collection systems using cryo-condensation [6–8]. This offers an alternative operational envelope by separating collection and thrust into two distinct phases as opposed to a continuous flow of gases through the system. Atmospheric gases are solidified during a collection phase before the intake is sealed with a valve. The solid air is then sublimated, generating the pressure required to feed the thruster using a more conventional feed system. This effectively decouples intake and thruster performances. To date, the collection-thrust cycle has not been demonstrated experimentally. This work outlines the design and development progress of a prototype collection and storage system to demonstrate the collection and thrust phases on ground.

1.1 Atmosphere-Breathing Electric Propulsion

The major sub-systems for ABEP are the intake and the thruster. The intake collects and delivers atmospheric gas to the thruster. Most proposed designs rely on passive intakes, which use the high orbital velocity and carefully designed ducts to both capture and compress the flow. This approach requires no power or moving parts and provides a continuous supply of propellant. However, performance is highly sensitive to local atmospheric conditions [9]. If the atmosphere is too dense, the intake may fail to provide sufficient mass flow for a given thruster power. If the atmosphere is too thin, the intake is unable to sufficiently compress the flow, preventing ionisation and therefore thrust. To balance these limitations, the intake outlet area can be adjusted: a larger outlet increases mass flow, while a smaller one increases gas density[4]. This results in a narrow operational envelope that is specific to the intake design[10].

The challenge is that local conditions in VLEO are far from stable. They vary widely with changes in solar activity, geomagnetic effects and local fluctuations. This leaves the system at the mercy of local changes and makes operating at the same altitude for long periods of time difficult. Thruster performance is likely to be impacted as most systems are optimised for specific pressures and flow rates, and operating under these fluctuating conditions can lead to reduced efficiency. Furthermore, during favourable conditions, more mass flow than is required than can be ingested. Although this is useful if additional thrust is required immediately, there is no option to store the gas and use it later.

1.2 Cryogenic propellant regeneration

Recent works have explored actively capturing and compressing ingested gases using cryogenic pumps[6–8]. Cryopumps are a form of capture pump: the gases are trapped

on a cold surface and held there until they can be released[11]. By cooling a surface to sufficiently cold temperatures it will act as a pump for gases around it: molecules that come into contact will stick to the surface and form a solid condensate. To release the gas the temperature of the surface is increased, allowing the captured gases to sublimate. These processes cannot occur simultaneously without complex mechanical systems to remove part of the condensate. Instead a valve is placed upstream from the pump to allow gas to be retained and provide the required feed pressure.

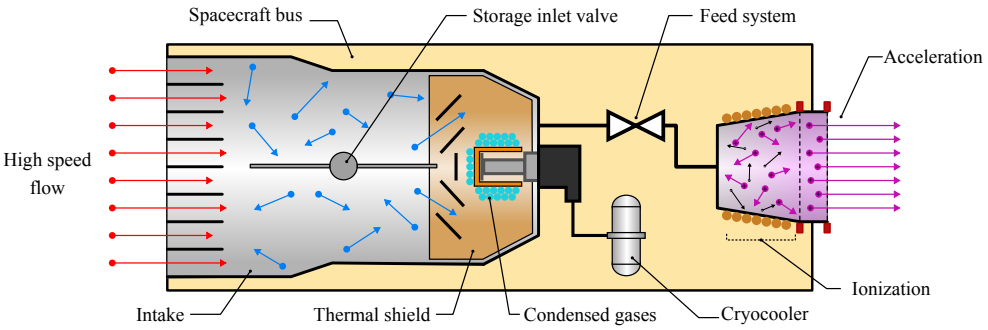


Fig. 1: Cryogenic propellant regeneration system architecture

The proposed use of cryopumps with ABEP is to place a pump at the outlet to a passive intake. A system system architecture with a single pump is shown in Figure 1. The pump collects the gases ingested by the passive intake during a preliminary collection phase. The system is cooled with a mechanical cryocooler. Then, once enough propellant has been captured, the inlet valve can be closed to create a pressure vessel. When the gas sublimes the pressure in the chamber rises and the gas can be used to feed the thruster through a feed system. In effect, this results in a propellant storage chamber that can be replenished using local gases.

This offers several advantages over a traditional intake system:

- The intake and thruster performances are decoupled: variations in local atmosphere do not vary the conditions inside the thruster.
- Propellant that is collected can be used at any time provided it can generate the required feed pressure. This enables the use of the system in regions of very low density such as at apogee during elliptical orbits.
- The higher supply pressure could allow the intake system to be connected to the thruster via a feed system and as opposed to a direct interface, allowing much more flexibility in bus design.
- The propellant can be fed through a mass flow controller and conventional feed lines, greatly simplifying thruster design and providing a constant and controllable mass flow at higher rates than is achievable through passive intakes alone.
- If the additional propellant beyond what is required can be stored as a surplus over time then it can be used to overcome regions of high drag or to perform other manoeuvres and possibly operations above VLEO.

During the collection phase the system produces no thrust. As a result, the spacecraft gradually decelerates and loses altitude while gathering propellant. When thrusting resumes, the system must not only counteract the drag force acting on the spacecraft, but also provide additional thrust to regain the lost altitude. The trade-off when compared to passive intakes is the additional power and complexity. A critical area of feasibility for such systems is the power required to cool the pump. While collecting, the pump surface must be cooled to cryogenic temperatures - about 20 K in the case of molecular nitrogen and oxygen [12]. Achieving and maintaining such temperatures is likely to require a multi-stage cryocooler. Collection must continue until the mass generated will produce enough pressure in the chamber to supply the thruster. During the thrust phase, the power requirement depends on how the collected condensate is managed. If all collected propellant is used up prior to the start of each collection phase then the pump acts as a simple pressure vessel. In this case the power can be delivered to either the thruster or the cooler without the need to power both. This provides a convenient power budget for the cooler: the required thruster power. This configuration prevents the need for additional bus power.

A successful cycle depends on many complex processes in the pump which are challenging to model accurately. The PHROST (Propellant Harvesting of Rarefied gases in-Orbit for Supplying electric Thrusters) test bed aims to investigate these processes experimentally. The work presented here represents the first design iteration of PHROST focusing on component selection and simulation of conditions during the collection phase.

2 Pump Design

The design of a cryopump largely depends on the gas that must be captured. The prototype is designed to pump the major constituents of sea level air: molecular nitrogen and oxygen. Due to the low quantity of lighter molecules found in air and the safety concerns of hydrogen regeneration, no adsorption stages were considered.

2.1 Pump Temperature

The condensation coefficient is the ratio of condensed particles to the total that are incident on the surface $\alpha_c = I_k/I_g$ [11]. To maximise the effectiveness of a pump, $\alpha_c = 1$ is ideal. This ideal case is achievable in practice for all gases except helium provided the surface temperature of the pump is low enough such that $p_k \gg p_f$ where p_k is the pressure surrounding the pump and p_f is the vapour pressure at the pump temperature. In the case of pumping N_2 and O_2, a common target is 20 K which corresponds to vapour pressures on the order of $1{\times}10^{-10}$ Pa and $\alpha_c = 1$ can be assumed for most practical scenarios.

Since the chamber walls could approach 300 K during summer room temperatures, an intermediate cooling stage between the storage chamber walls and the pump surface is likely required to reduce the thermal load. It is common practice for pumps to have an intermediate stage at around 80 K.

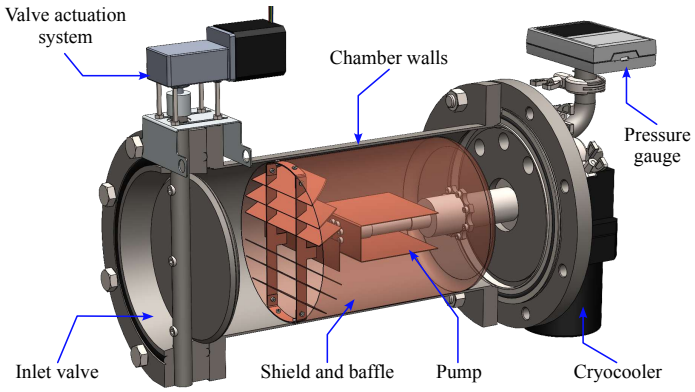


Fig. 2: Configuration and major components of PHROST testbed assembly

2.2 Component selection

The choice of primary components for the test bed were driven by systems with the potential for high development cost. Most notably the cryocooler and the inlet valve. To accelerate development, existing solutions from the vacuum industry were used for the inlet, chamber walls and cooler.

Figure 2 shows the major components of the PHROST test bed assembly consisting of the following major sub-systems and components:

- *Cryocooler:* The Oxford Cryosystems 2/9 two stage Gifford-McMahon cooler was chosen for its small form factor, compatibility with submergence in vacuum, and support for fine temperature control. The nominal refrigeration performance is a first stage providing 9 W at 77 K and a second stage providing 2 W at 20 K.
- *Inlet valve:* An Edwards QSB160 butterfly valve. Provides up to 1 bar pressure difference while closed and can be modified for working with a custom actuation system. Additionally butterfly valves are a good candidate to represent an on-orbit system as they minimise the theoretical spacecraft frontal area when compared to gate valves.
- *Chamber walls:* Custom manufactured ISO 160 tube section and rear flange with ports for mounting instrumentation and feed lines.
- *Valve actuation system:* A custom build remote actuation system for operating the inlet valve in vacuum.
- *Instrumentation:* The rear flange is fitted with three KF16 flanges for mounting a Swagelok connector, pressure gauge and temperature monitor feed-through.

2.3 Shield and Baffle Design

The purpose of the shield is to minimise heat transfer to the pump while retaining as much molecular conductance as possible [11]. The effects of thermal radiation play a significant role if the chamber walls are room temperature. To obstruct the line of sight between the high temperature components and the pump surface, it is common

to use an array of overlapping baffles. The degree of overlap and their shape is usually the result of a trade-off between molecular transmission probability from the pump inlet to the pump surface, and the baffle's radiation transmission. Figure 3 shows the shielding effect of baffles in the configuration used for PHROST.

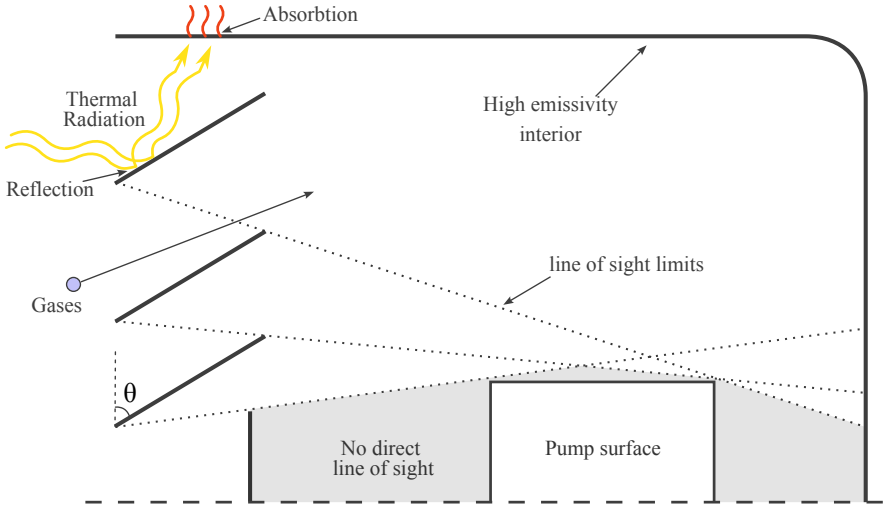
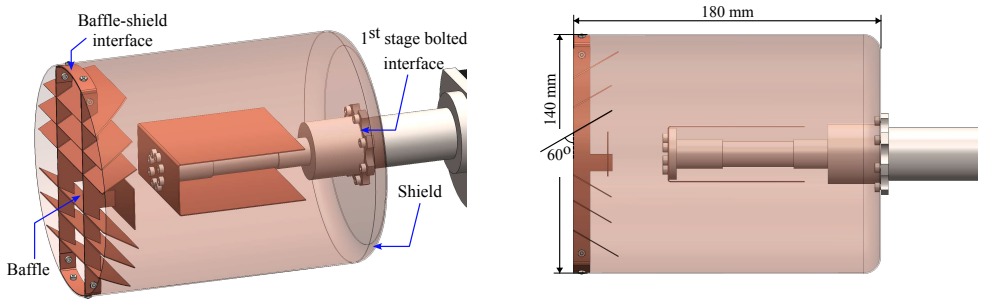


Fig. 3: Cryopump baffle and shield configuration and design principle

To maximise flow into the pump the shield radius should be almost as large as the inlet to the chamber. To maximise transmission through the baffle a louvre type was chosen, which can provide high flow rates at the cost of higher radiation transmission [11]. The baffle and shield designs are shown in figure 4.



(a) (b)

Fig. 4: PHROST thermal radiation shield, (a) Baffle and shield assembly, (b) Shield assembly dimensions

The louvres are held in place using slotted panels that are bolted to the shield. The shield is bolted directly to the first stage of the cooler. Further design considerations for both the shield and baffle were as follows:

- A louvre angle of $\theta = 60°$ is recommended to maximise transmission probability [11]. The louvre aspect ratio (taken as the ratio between the inlet radius and louvre depth) should be maximised for the same reason. Higher ratios results in a higher number of louvre panels and increased manufacturing complexity. Though several iterations a quantity of 7 was chosen based on manufacturing capabilities and the aspect ratio was then chosen to fully occlude the pump surface.
- The positions of the louvres aim to prevent any direct line of sight to the pump surface while maximising the lines of sight into the shield volume. In theory this maximises the conductance through the baffle.
- The shield and baffle material should have a high thermal conductivity to reduce cooldown times, have a low emissivity to reflect radiation from the surrounding chamber walls, and be suitable in vacuum. High purity copper was chosen for all cooled components.
- Minimising the mass of the shield reduces cooldown times as less thermal energy must be removed by the first stage of the cooler. For PHROST, this manifests as an improvement in cycle efficiency as less time is spent in the transition between thrust and collection phases. Based on preliminary material rigidity tests the target thickness for all parts is 0.6 mm.

A summary of design parameters for the shield are detailed in Table 1 and Table 2.

Table 1: Thermal radiation shield design parameters

Parameter	Value
Outer diameter	140 mm
Length	180 mm
Thickness	0.60 mm
Material	C101
Surface Area (Including Baffle)	0.23 m^2
Estimated Mass	0.49 kg

Table 2: Shield baffle design parameters

Parameter	Value
Louvre angle	60°
Louvre Aspect Ratio	5
Louvre Panels	7
Louvre thickness	0.6 mm
Material	C101
Estimated Mass	0.14 kg

2.4 Pump Surface Design

The choice of a louvre type baffle restricts the feasible dimensions of the pump surface to the region behind the baffle that avoids any direct radiation impingement. A simple U shaped sheet metal panel was designed to fit within the area shaded by the louvres as shown in Figure 3. The surface is mounted on the cooler second stage. Figure 5 details the pump surface design. A summary of the pump surface design parameters are shown in Table 3.

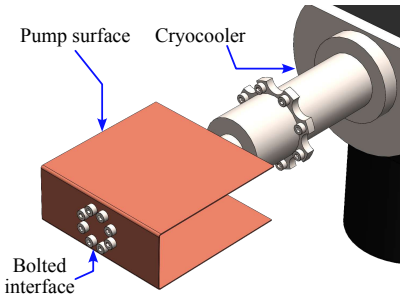


Fig. 5: Pump surface design

Table 3: Pump surface design parameters

Parameter	Value
Width	80 mm
Length	80 mm
Thickness	0.6 mm
Surface area	0.03 m^2
Material	C101
Mass	81 g

2.5 Pump inlet conditions

The construction of a rarefied gas intake is relatively simple compared to other components in an ABEP system. However testing the intake by simulating atmospheric conditions at orbital velocity is far more complex. Previous work from Andreussi et al [5] simulated incoming flow conditions by feeding a hall effect thruster with a mixture of N_2 and O_2. Pressures below $2{\times}10^{-4}$ mbar were achieved with a mean flow velocity of 9.12 km/s that supplied an incoming flow of 5 mg/s to the intake. The development of such a system was deemed to be outside the scope and available costs for the project. Instead of simulating a full intake system, the design pressure of the pump was assumed to be the fully thermalised conditions after a typical intake. With this

assumption the chamber can be pumped to the design pressure and then kept at this pressure during the collection phase using a steady supply of gas.

To determine a working pressure for the chamber, the flow conditions for a simple representative intake were calculated with molecular flow analysis and a local atmosphere model. NRLMSIS 2.1[13] was used to compute the local conditions under moderate solar activity in a circular orbit at 240 km above Earth's surface and averaged based on a regular 100x100 grid of latitudes and longitudes. Relevant outputs from the model are shown in table 4.

Table 4: Representative atmospheric conditions at 240 km

Parameter	Value
Mass Density	7.02×10^{-11} kg m^{-3}
Number Density (n_∞)	2.20×10^{15} m^{-3}
Temperature (T_∞)	920 K
Number Density of Nitrogen Species*	5.88×10^{14} m^{-3}
Number Density of Oxygen Species*	1.60×10^{15} m^{-3}
Mean Molecular Mass ($\bar{m}$)	3.20×10^{-26} kg
Pressure	2.79×10^{-7} mbar

* *Sum of number densities for N_2, N, O_2, O, and Anomalous Oxygen*

An important parameter for intake performance is ratio between the flow velocity V_∞ and the mean thermal velocity of the gas, known as the speed ratio [9]. The speed ratio indicates the degree to which the flow is collimated with respect to the intake. For a circular orbit $V_\infty = \sqrt{\mu_E/r}$ where μ_E is Earth's gravitational parameter and the orbital radius at 240 km above Earth's average radius is $r = 6371$ km. Under the representative conditions used for the design point a speed ratio of $S_\infty = 8.71$ was determined using equation 1 for $V_\infty = 7764$ m/s.

$$S_\infty = V_\infty \sqrt{\frac{\bar{m}}{2kT_\infty}} \tag{1}$$

Where k is the Boltzmann constant. The intake was modelled as a series of symmetrical ducts on the front face of the spacecraft that are aligned with the incoming flow. The flow conditions inside the intake can be determined analytically if the conditions through and after the ducts are free molecular and fully thermalised to the temperature of the walls T_w [4, 9, 14]. The density ratio ν across the intake can be determined with equation 2.

$$\nu = 2\sqrt{\pi} S_\infty \sqrt{\frac{T_\infty}{T_w}} \frac{\tau_{d,i}}{\tau_{d,o} + \frac{A_s}{A_i}\tau_s} \tag{2}$$

The transmission probabilities into and out of the intake ducts, $\tau_{d,i}$ and $\tau_{d,o}$, were determined analytically using the method from Hughes and De Leeuw [15]. Further

details on this method and its validation are outlined in Appendix A. For the representative intake, a duct aspect ratio of $D_d/L_d = 0.22$ was chosen for an inlet area of $A_i = 0.02$ m^2. The intake outlet area was assumed to be the same as the pump inlet valve $A_s = 0.0172$ m^2. The transmission probability that a molecule will travel from the intake outlet to the pump surface was found to be $\tau_s = 0.2674$ based on molecular flow analysis in section 2.6. The transmission probability is purely a function of geometry, so a random inlet density was used prior to determining the full inlet flow conditions. Finally, the gas in the system was assumed to be an ideal gas when determining the pressure from the calculated number density.

$$p_i = \nu n_\infty k T_w \tag{3}$$

The flow conditions used as inlet conditions for the pump are shown in table 5. The intake pressures calculated under representative conditions on orbit will be used as the vacuum chamber target pressure during experiments.

Table 5: Representative inlet conditions

Parameter	Value
Density ratio	88.16
Intake number density	1.93×10^{17} m^{-3}
Intake wall temperature	300 K
Intake pressure	8.01×10^{-6} mbar

2.6 Molecular Flow Analysis

The flow conditions in the chamber during collection and the pump transmission probabilities were simulated using Molflow+ [16]: A Test-particle Monte-Carlo (TPMC) solver developed at CERN for UHV systems such as cryopumps. TPMC solves the conductance in the system by modelling the trajectories of particles, representing parcels of many real molecules, from their source to the pump surface. Trajectories are modelled using ray-tracing algorithms to propagate the location of molecules in the pump volume. Collisions with walls are modelled as diffuse reflections using Knudsen's cosine law. Wall collisions are used to determine physical quantities like impingement rate, pressure and density. Intermolecular collisions are not modelled and as such results can only considered valid under free molecular flow conditions. A simplified simulation geometry, shown in Figure 6, was created for both the molecular flow simulations and later heat transfer analysis.

The inlet was treated as an outgassing surface with a sticking factor of one to remove molecules that return back through the inlet. The outgassing rate at the inlet facet in Molflow+ is the product of the pressure and the volume flow rate at the face, where volume flow rate is the product of area and velocity $Q = vA$. These parameters were taken to be the intake pressure p_i and the volume flow rate into the pump Q_s respectively. It was assumed that the flow conditions leaving the intake would be

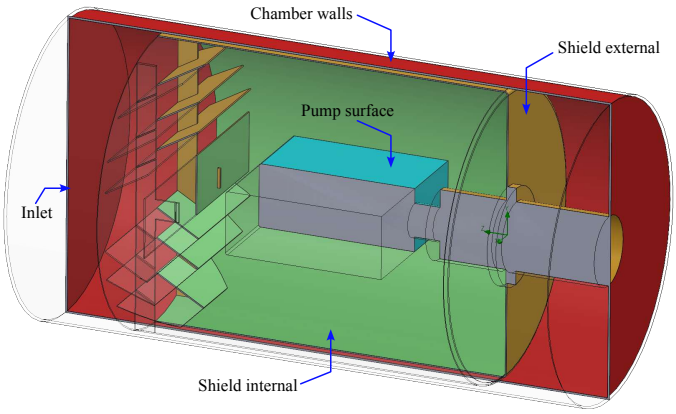


Fig. 6: Simplified simulation geometry used for Molflow+ and radiation heat transfer analysis

thermalised to the wall conditions. Therefore the velocity at the pump inlet v_s can be taken to be the mean normal component of velocity relative to a face at T_w, as shown in Equation 4 [11].

$$v_s = \bar{v}_w/4 = \sqrt{\frac{kT_w}{2\pi\bar{m}}} \tag{4}$$

The outgassing rate on the inlet facet can then be determined using the flow conditions inside the intake in Table 5 with equation 5.

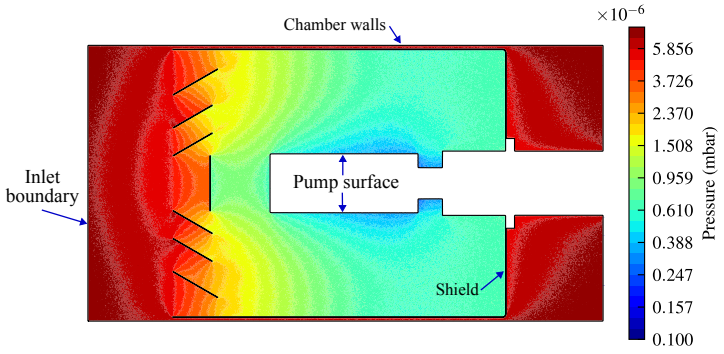
$$p_i Q_s = \frac{1}{4} p_i \bar{v}_w A_s = p_i A_s \sqrt{\frac{kT_w}{2\pi\bar{m}}} \tag{5}$$

Where the product of intake pressure p_i and volume flow rate into the pump Q_s is the outgassing rate. The pump surface was assumed to have a sticking factor of 1. A summary of boundary conditions are shown in Table 6.

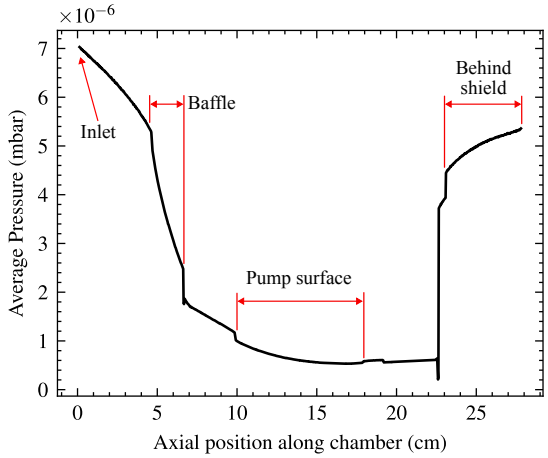
Table 6: Molecular flow simulation boundary conditions

Parameter	Inlet	Chamber Walls	Shield	Pump Surface
Temperature (K)	300	300	80	20
Outgassing (mbar l s^{-1})	1.98×10^{-2}	0	0	0
Sticking Factor	1	0	0	1

The simulation was run for approximately 2×10^8 desorption events after which the statistical uncertainty was sufficiently small. Details of the convergence criteria are shown in Appendix B and simulation methodology is verified against Clausing's solution to finite cylinders in Figure A1a. The transmission probability between the



(a)



(b)

Fig. 7: Molflow+ chamber pressure results for the boundary conditions in table 6. (a) Pressure field in the YZ plane, (b) Average pressure along Z axis.

pump inlet and the pump surface was found to be $\tau_s = 0.2674$. Figure 7 shows the pressure flow-field and pressure averaged along the central axis of the chamber.

As expected the lowest pressure is found at the pump surface where molecules are removed from the domain. The highest pressure is seen at the corners of the inlet at nearly the intake pressure. A summary of the expected pump conditions during collection are shown in Table 7. The pressures and densities are average values across the facets in the geometry mesh.

2.7 Heat Transfer Analysis

Under steady state conditions the required refrigeration power for each stage of the pump is the sum of heat flow rates acting on the stage [11]. Equations 6 and 7 represent the heat loads on the first and second stages respectively. For both stages it was

Table 7: Molecular flow simulation result summary

Net result	Value		
Transmission Probability	0.2674		
Regional Result	**Inlet**	**Shield (External)**	**Pump Surface**
Pressure (mbar)	6.33×10^{-6}	5.39×10^{-6}	4.14×10^{-7}
Neutral Density (m^{-3})	1.93×10^{17}	2.58×10^{17}	4.08×10^{16}

Table 8: Radiation heat transfer simulation boundary conditions and net heat loads

Boundary Face	Emissivity	Temperature (K)	Net Load (W)
Inlet	0.1	300	-0.637
Chamber Walls	0.1	300	-2.476
Shield (External)	0.05	80	1.743
Shield (Internal)	0.9	80	1.296
Pump Surface	0.9	20	0.067

assumed that the cooler would provide sufficient thermal isolation to negate the effects of solid conduction.

$$\dot{Q}_{sh} = \dot{Q}_{rs} + \dot{Q}_{gas} \tag{6}$$

The cooler capacity required for the shield $\dot{Q}_{sh}$ is the sum of radiation heat transfer $\dot{Q}_{rs}$ and gas conduction heat transfer $\dot{Q}_{gas}$ experienced by the shield and baffle.

$$\dot{Q}_{p} = \dot{Q}_{rp} + \dot{Q}_{cond} \tag{7}$$

While the cooler capacity required for pump stage $\dot{Q}_{p}$ is the sum of radiation heat transfer $\dot{Q}_{rp}$ and the heat load due to condensation at the pump surface $\dot{Q}_{cond}$. The effect of thermal radiation was evaluated for shield and pump surface designs using surface-to-surface radiation heat transfer analysis in the Solidworks Flow Simulation package [17].

The emissivities of the surfaces in the pump play a vital role in controlling the heat transfer in the pump. Minimising the emissivity will results in lower heat transfer and reduce power requirements. For a mechanically polished copper surface at cryogenic temperatures an emissivity of 0.05 is achievable [18]. Although this can also be assumed for the pump surface at the start of the collection phase, as a condensate builds on the pump surface the emissivity will quickly increase towards $\epsilon_p \approx 0.9$ [11]. This in turn increases the pump heat load and can compromise effective layer growth on the pump surface. To mitigate this effect it is common to apply a high emissivity coating to the inside of the baffle and shield to absorb reflecting rays as shown in figure 3. Table 8 shows the temperatures and emissivities assumed for each surface along with the resulting net heat loads.

The heat load due to gas conduction was estimated using the pressure measurements from the molecular flow analysis using recommended values and relations from

Haefer [11]. Gaseous conduction was considered between the chamber wall at temperature $T_w = 300$ K and the shield exterior walls at $T_{sh} = 80$ K. The heat transfer rate $\dot{Q}_{gas}$ was calculated at the pressure surrounding the external walls of the shield p_{sh} using equation 8.

$$\dot{Q}_{gas} = \frac{\kappa + 1}{\kappa - 1} \left(\frac{R}{8\pi M T_n} \right)^{1/2} a A_{sh} p_{sh} (T_w - T_{sh}) \tag{8}$$

Where κ is the heat capacity ratio of the gas at reference temperature T_n, M is the molar mass of the gas, and R is the universal gas constant. The effective accommodation coefficient a can be estimated with equation 9 using approximate values for the thermal accommodation of the wall surface a_w =0.8 and the shield surface $a_{sh} = 1$.

$$a = [a_{sh}^{-1} + A_{sh}(a_w^{-1} - 1)/A_w]^{-1} \tag{9}$$

During the collection phase it is assumed that the fraction of particles incident on the pump surface is $\alpha = 1$ if the temperature of 20 K can be achieved. Under these conditions the amount of molecules that do not condense or are re-captured can be ignored and the condensation heat load $\dot{Q}_{cond}$ can be determined using equation 10.

$$\dot{Q}_{gas} = \alpha A_k p_i (\bar{v}_n / 4) \Delta H / R T_n \tag{10}$$

Where ΔH is the enthalpy change during condensation from 80 K to 20 K for the gas, A_k is the surface area of the pump and p_i is the pressure inside the shield close the the pump surface. The average thermal velocity of the gas $\bar{v}_n$ at the reference temperature $T_n = 293$ K was determined assuming a Maxwell velocity distribution with equation 11.

$$\bar{v}_n = \left(\frac{8 k T_n}{\pi \bar{m}} \right)^{1/2} \tag{11}$$

Table 9 details the assumed chamber conditions and constants derived from literature. Using equations 6 and 7 the sum of heat loads were used to estimate the required refrigeration power at each stage as shown in Table 9.

Table 9: Molecular heat transfer parameters

Parameter	Value	Notes
$\frac{\kappa+1}{\kappa-1}\left(\frac{R}{8\pi M T_n}\right)^{1/2}$	$1.15\,\mathrm{W\,m^{-2}\,Pa^{-1}\,K^{-1}}$	Experimental values for N2*
$\Delta H(80\,\mathrm{K} \rightarrow 20\,\mathrm{K})/RT_n$	3.70 $\mathrm{W(Pa\,m^3\,s^{-1})^{-1}}$	Experimental values for N2*
T_n	293 K	Reference temperature*
a	0.81	Accommodation coefficient from eq. 9

* Values taken from recommendations in Haefer[11]

Table 10: Refrigeration loads and comparison to cooler capacity

Source	Stage 1 (80 K)	Stage 2 (20 K)
Radiation	3.046 W	0.067 W
Gas Conduction	1.165×10^{-2} W	-
Condensation	-	5.557×10^{-4} W
Net Thermal Load	3.058 W	0.068 W
Cooler Capacity	9 W	2 W

3 Prototype Development Progress & Experimental Setup

Figures 8 shows the experimental setup for PHROST. The system is integrated with a larger 1 m by 0.6 m diameter chamber which acts as the source for the thermalised inlet flow. The chamber's primary pump has a pumping speed of 1900 L/s for N_2. The chamber has a typical ultimate pressure of 1×10^{-6} mbar, allowing low pressures to be achieved during both collection and thrust phases.

Figure 9 shows a diagram of the experimental setup. Since PHROST acts as a pump, the inlet pressures are reduced during the collection phase. To maintain the correct inlet pressures, an atmosphere admission system line was added to inject a controlled supply of gas. This also adds the ability to use custom mixtures of nitrogen and oxygen with low moisture content to avoid ice build-up. The temperature of the second stage is monitored via a platinum resistance sensor mounted on the pump surface. Cooled copper components, shown in Figure 10, were mounted using indium gaskets, which provide good thermal conductivity while remaining ductile at cryogenic

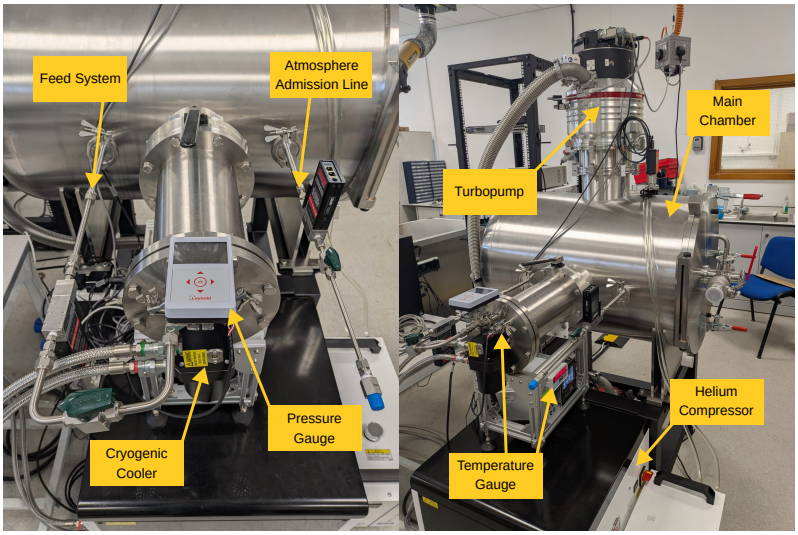


Fig. 8: PHROST experimental setup

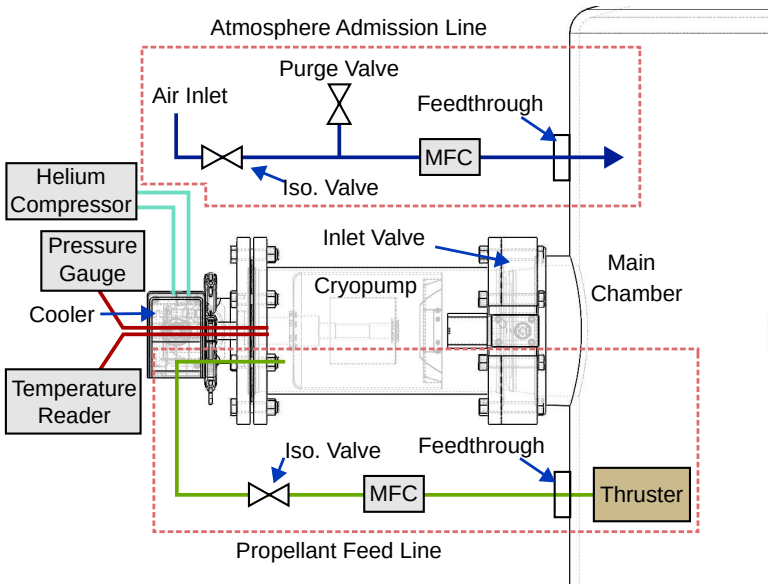


Fig. 9: PHROST experimental setup diagram

temperatures. During thrust phases, the inlet valve isolates the pump volume from the main chamber, allowing the air to be fed back into the main chamber through a thruster. A target feed pressure after collection of 50 mbar was chosen based on feed system design requirements from previous work [7].

At present, the PHROST setup is undergoing assembly integration and testing for major subsystems.

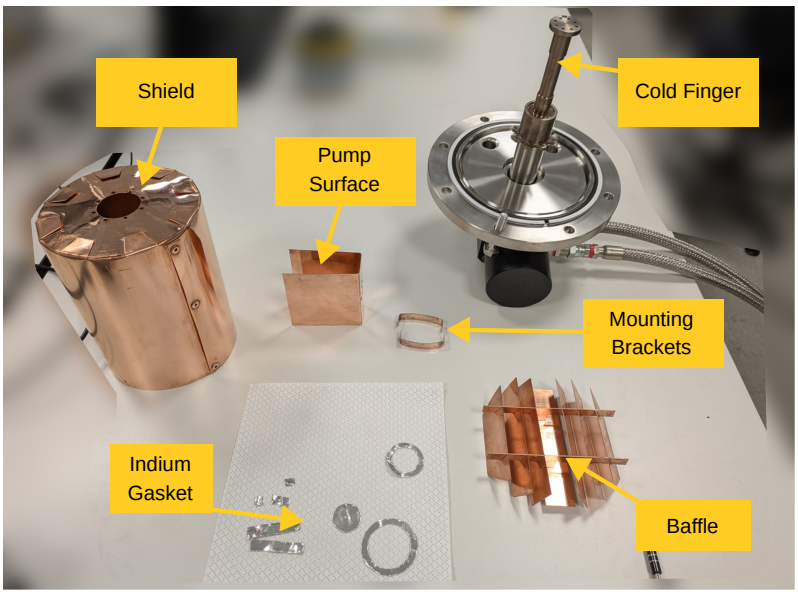


Fig. 10: PHROST cooler mounted components

4 Conclusion

In conclusion the design process for the PHROST prototype has been presented. A methodology based on established practices in the vacuum industry was used to develop a cryopump system that meets the requirements to test the collection and thrust cycle. A target temperature of 20 K was found to meet the requirements for the capture of nitrogen and oxygen. Components for the inlet, storage chamber walls, and cooling system were chosen based on feasible off-the-shelf solutions. Then a custom shield and pump surface were designed within cooling constraints of the chosen cooler.

To test the system at representative conditions that would be experienced in orbit, a simple methodology was adopted: Firstly the NRLMSIS 2.1 atmospheric model was used to estimate local conditions at 240 km. Then, a simple analytical model for a passive intake stage prior to the storage system was used to determine the inlet conditions during collection. This resulted in a design inlet pressure of 8.01×10^{-6} mbar. To simulate collection under these conditions the vacuum chamber will be kept at this pressure.

To estimate the flow conditions within the pump during collection, Molflow+ was used to perform TPMC simulations. For the geometry presented a transmission probability of $\tau_s = 0.2674$ was determined. The pressures inside the pump were determined using inlet conditions determined in section 2.5. The results were used to estimate the heat loads on both stages for the collection phase: 3.058 W for the 80 K shield stage and 0.068 W for the 20 K pump stage. Both estimates fell within the limitations of the chosen cryocooler that would be used for experiments. Finally the experimental setup was presented at its current development stage.

Declarations

Author contributions

All research content and Manuscript writing: C.L. Manuscript review and supervision E.G. Supervision: S.H.

Funding

This work was financially supported by the European Space Agency in a co-funded PhD project with Cranfield University under the "Open Space Innovation Platform".

Competing Interests

The authors declare no competing interests.

Data availability

The data that support the findings of this study are available from the corresponding author upon reasonable request.

Appendix A Intake transmission probabilities

The intake was assumed to be a collection of cylindrical ducts of equal length and diameter such that the sum of their cross sectional areas was equal to the intake frontal area. This simplification is used to determine the transmission probability through the ducts analytically: a common practice with passive intake analysis [4, 9, 14].

Hughes' method was used to calculate the transmission probabilties assuming an angle of attack of $\alpha = 0°$ for speed ratios of $S > 0$ into the intake. For flow returning back through the ducts at $S = 0$ the calculation simplifies to Clausing's case [19].

The calculated transmission probabilities, used to determine the density ratio, where compared to results in Parodi et al, shown in A2.

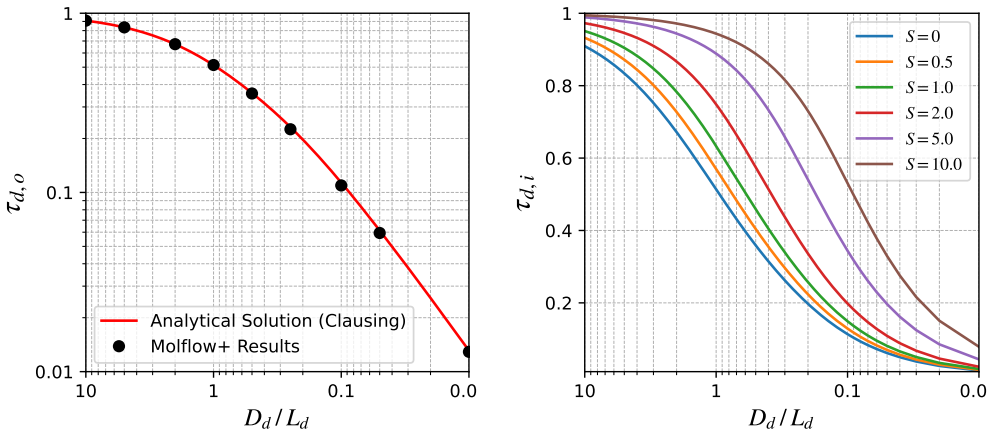


Fig. A1: Transmission probabilities for varying duct diameter ratio D_d/L_d, (a) Transmission probabilities leaving the intake under $S = 0$ condition using Clausing method [19], compared to Molflow+ results, (b) Transmission probability into ducts with increasing speed ratio using Hughes' method [15]

.

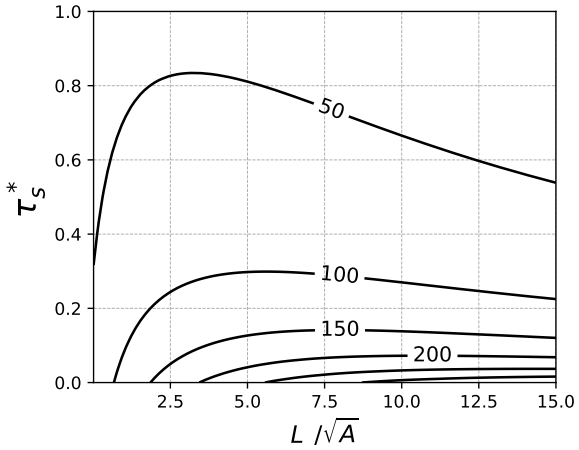


Fig. A2: Results of Density ratios for varying outlet transmissivity and duct aspect ratios using Parodi's method [9].

Appendix B Molflow+ convergence

The uncertainty within a TPMC simulation is reduced with increasing particle injections. A common criteria to assess is the uncertainty in the transmission probability which can be taken as $\pm 2\sigma_{\tau_s}$ where the standard deviation σ_{τ_s} follows a binomial distribution [20, 21].

$$\sigma_{\tau_s} = \sqrt{\frac{\tau_s(1-\tau_s)}{N}} \tag{B1}$$

Where N is the number of injected particles. A statistical uncertainty of below $\tau_s \pm 0.001$ was quickly reached with every simulation due to the small and relatively simple geometry. This uncertainty was found to be in good agreement with comparisons to results from Clausing, shown in Figure A1a. Figure B3 shows the standard deviation throughout the final simulation which resulted in an uncertainty of $\tau_s \pm 0.00017$.

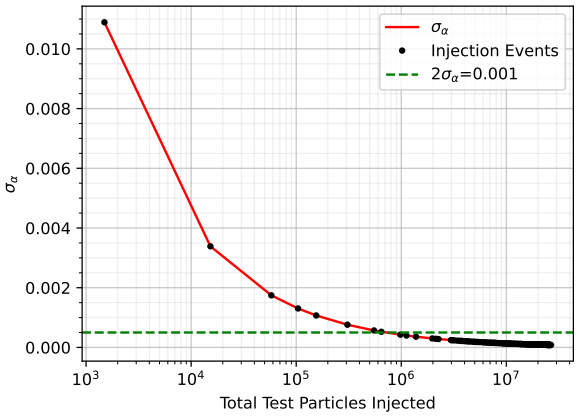


Fig. B3: Standard deviation during simulation with increasing total injected particles.

Appendix C Heat transfer simulation verification and mesh independence

Heat transfer simulation methodologies were verified against analytical solutions for radiative heat transfer between concentric cylinders. The view factors between finite concentric cylinders are determined analytically [22]. Equation C2 shows the conventional relation for heat transfer between two diffuse bodies.

$$Q_{1\to2} = \frac{\sigma\left(T_1^4 - T_2^4\right)}{\frac{1-\varepsilon_1}{\varepsilon_1 A_1} + \frac{1}{A_1 F_{12}} + \frac{1-\varepsilon_2}{\varepsilon_2 A_2}} \tag{C2}$$

Table C1: Heat transfer rate concentric cylinder verification

	Outer cylinder (2)	Inner cylinder (1)
Radius	80 mm	20 mm
Temperature (T)	80 K	20 K
Emissivity (ϵ)	0.1	0.9
Length	200 mm	200 mm
Surface Area (A)	0.1 m^2	0.025 m^2
View factor* (F_{12})	0.201	
$\dot{Q}_{1\to2}$ (Analytical)	-0.00789 W	
$\dot{Q}_{1\to2}$ (Simulation)	-0.00797 W	

* View factor from outer cylinder to inner cylinder calculated with view factor relations for concentric circular cylinders of the same length [22].

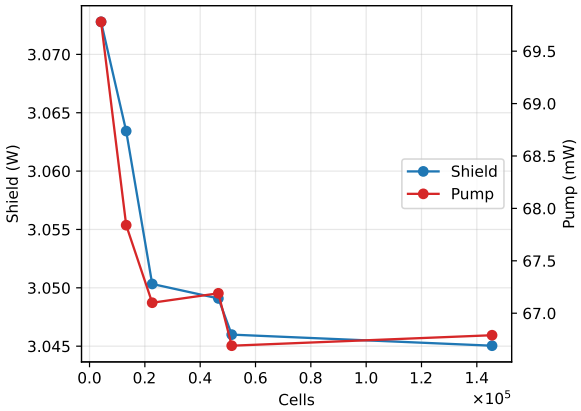


Fig. C4: Mesh cell count against pump and shield refrigeration loads.

To ensure the geometry mesh was adequate for representing the real pump geometry, a mesh independence study was performed. Results for the value of required cooling load to both the pump and shield are shown in C4 against total cell count.

References

[1] Crisp, N.H., Roberts, P.C.E., Livadiotti, S., Oiko, V.T.A., Edmondson, S., Haigh, S.J., Huyton, C., Sinpetru, L.A., Smith, K.L., Worrall, S.D., Becedas, J., Domínguez, R.M., González, D., Hanessian, V., Mølgaard, A., Nielsen, J., Bisgaard, M., Chan, Y.-A., Fasoulas, S., Herdrich, G.H., Romano, F., Traub, C., García-Almiñana, D., Rodríguez-Donaire, S., Sureda, M., Kataria, D., Outlaw, R., Belkouchi, B., Conte, A., Perez, J.S., Villain, R., Heißerer, B., Schwalber, A.: The benefits of very low earth orbit for earth observation missions **117**, 100619 https://doi.org/10.1016/j.paerosci.2020.100619

[2] Nishiyama, K.: Air breathing ion engine concept. In: 54th International Astronautical Congress of the International Astronautical Federation, the International Academy of Astronautics, and the International Institute of Space Law. American Institute of Aeronautics and Astronautics. https://doi.org/10.2514/6.IAC-03-S.4.02

[3] Di Cara, D., Amo, J., Santovincenzo, A., Carnicero Dominguez, B., Arcioni, M., Caldwell, A., Roma, I.: RAM electric propulsion for low earth orbit operation: An ESA study. In: 30th International Electric Propulsion Conference, vol. 21, p. 22

[4] Barral, S., Cifali, G., Albertoni, R., Andrenucci, M., Walpot, L.: Conceptual design of an air-breathing electric propulsion system. In: 34th International Electric Propulsion Conference and 6th Nano-satellite Symposium

[5] Andreussi, T., Ferrato, E., Giannetti, V., Piragino, A., Paissoni, C.A., Cifali,

G., Andrenucci, M.: Development status and way forward of SITAEL's air-breathing electric propulsion engine. In: AIAA Propulsion and Energy 2019 Forum. American Institute of Aeronautics and Astronautics. https://doi.org/10.2514/6.2019-3995

[6] Leslie, C.F.: A Novel Cryogenic Storage Solution for Atmosphere-Breathing Electric Propulsion Systems. https://doi.org/10.13140/RG.2.2.10965.08160 . https://dspace.lib.cranfield.ac.uk/items/58839a86-2104-4849-a99e-db259c3b458e

[7] Leslie, C., Grustan-Gutiérrez, E., Hobbs, S.: Towards experimental demonstration of cryogenic propellant regeneration for atmosphere-breathing electric propulsion. In: 10th Edition of the Space Propulsion Conference, Bari, Italy (2026)

[8] Moon, G., Yi, M., Jun, E.: Design and operational concept of a cryogenic active intake device for atmosphere-breathing electric propulsion **151**, 109300 https://doi.org/10.1016/j.ast.2024.109300

[9] Parodi, P., Le Quang, D., Bariselli, F., Boccelli, S., Alsalihi, Z., Magin, T.: Study of a collector-intake system for VLEO air-breathing platforms. In: International Conference on Flight Vehicles, Aerothermodynamics and Re-entry Missions and Engineering (FAR)

[10] Tisaev, M., Ferrato, E., Giannetti, V., Paissoni, C.A., Baresi, N., Lucca Fabris, A., Andreussi, T.: Air-breathing electric propulsion: Flight envelope identification and development of control for long-term orbital stability **191**, 374–393 https://doi.org/10.1016/j.actaastro.2021.11.011

[11] Haefer, R.A.: Cryopumping: Theory and Practice. Monographs on Cryogenics. Clarendon Press. https://books.google.co.uk/books?id=wHaLAAAAIAAJ

[12] Day, C.: Basics and applications of cryopumps. In: CAS - CERN Accelerator School: Vacuum in Accelerators, pp. 241–274. CERN. https://doi.org/10.5170/CERN-2007-003.241

[13] Emmert, J.T., Jones, M., Siskind, D.E., Drob, D.P., Picone, J.M., Stevens, M.H., Bailey, S.M., Bender, S., Bernath, P.F., Funke, B., Hervig, M.E., Pérot, K.: NRLMSIS 2.1: An empirical model of nitric oxide incorporated into MSIS **127**(10), 2022–030896 https://doi.org/10.1029/2022JA030896

[14] Binder, T., Boldini, P.C., Romano, F., Herdrich, G., Fasoulas, S.: Transmission probabilities of rarefied flows in the application of atmosphere-breathing electric propulsion. In: 30th International Symposium on Rarefied Gas Dynamics: RGD 30, p. 190011. https://doi.org/10.1063/1.4967689

[15] Hughes, P.C., De Leeuw, J.H.: Theory for the free molecule impact probe at an angle of attack. In: Leeuw, J.H. (ed.) Rarefied Gas Dynamics: Fourth Symposium. Advances in Applied Mechanics, vol. 1, pp. 653–676. Academic Press

[16] Kersevan, R., Ady, M.: Recent developments of Monte-Carlo codes Molflow+ and Synrad+. In: Boland, M., Tanaka, H., Button, D., Dowd, R., Schaa, V.R.W., Tan, E. (eds.) Proceedings of the 10th International Particle Accelerator Conference (IPAC'19), pp. 1327–1330. JACoW Publishing. https://doi.org/10.18429/JACOW-IPAC2019-TUPMP037

[17] Dassault Systèmes: SOLIDWORKS 2025. https://www.solidworks.com

[18] Frolec, J., Králík, T., Musilová, V., Hanzelka, P., Srnka, A., Jelínek, J.: A database of metallic materials emissivities and absorptivities for cryogenics **97**, 85–99 https://doi.org/10.1016/j.cryogenics.2018.12.003

[19] Clausing, P.: The flow of highly rarefied gases through tubes of arbitrary length **8**(5), 636–646 https://doi.org/10.1116/1.1316379

[20] Gómez-Goñi, J., Lobo, P.J.: Comparison between Monte Carlo and analytical calculation of the conductance of cylindrical and conical tubes **21**(4), 1452–1457 https://doi.org/10.1116/1.1568746

[21] Kersevan, R.: Analytical and numerical tools for vacuum systems. In: Brandt, D. (ed.) CAS - CERN Accelerator School: Vacuum in Accelerators. CERN. https://doi.org/10.5170/CERN-2007-003.285

[22] ECSS Secretariat: Thermal Design Handbook – Part 1: View Factors. European Cooperation for Space Standardization. European Cooperation for Space Standardization. https://ecss.nl/wp-content/uploads/2011/12/ECSS-E-HB-31-01_Part1A.pdf